Hyperspectral Imaging of Kaposi's Sarcoma for Disease Assessment and Treatment Monitoring

David Hattery, Moinuddin Hassan
Laboratory of Integrative and Medical Biophysics, Building 12a, Room 2041
National Institutes of Health, Bethesda, MD 20892-5626
hattery@ieee.org, hassanm@mail.nih.gov

Stavros Demos
Lawrence Livermore National Laboratory
PO Box 808, L-411, Livermore, CA 94551
demos1@llnl.gov

Amir Gandjbakhche
Laboratory of Integrative and Medical Biophysics, Building 12a, Room 2041
National Institutes of Health, Bethesda, MD 20892-5626
amir@helix.nih.gov

Abstract

Light spectroscopic methods are critical to advances in molecular characterization of disease processes. However, these methods have been limited to in-vitro or cell culture studies. In fact, strong scattering in almost all tissue types causes dispersion of the photons paths which results in poor localization and resolution. Hence, quantitative analysis of spectral data obtained from structures below the tissue surface requires accounting for scattering which affects both the penetration of the photons and the path length over which the photons will be subject to molecularly speci£c absorption.

The goal of much current research is to non-invasively obtain diagnostically useful molecular information from embedded sites. We have designed and built a six-band multi-spectral NIR imaging system which we have used on patients with highly vascularized tumors in the skin called Kaposi's Sarcoma. The imaged lesions are undergoing treatment with experimental anti-angiogenesis drugs that are designed to reduce blood ¤ow and hence growth of the tumors. The NIR data is combined with both 3-5 micron and 8-12 micron infrared images, obtained of the same tumors, which are used to identify thermal signatures of blood volume, as well as three-band visible wavelength data which show the visible extent of the lesions.

We have developed a layered model of the skin in which speci£c analytes exist in speci£c layers. The spectral signatures of analytes such as oxy- and deoxy-hemoglobin are known. To obtain information on the concentration of those analytes in the tissue, however, the diffuse re¤ectance NIR images from the patients must be corrected for scattering. The scattering is modeled using analytical solutions developed from a random walk model of photon migration in turbid media. When the hyperspectral patient data is £t to the model, physiologically related parameters, such as to blood volume and oxygenation, are obtained. This provides clinically important data that may be used by the physician for evaluations of drug effectiveness, disease assessment and patient treatment monitoring.

1 Introduction

We have designed a spectral imager that captures images at six wavelengths in the NIR (700, 750, 800, 850, 900, and 1000 nm). The NIR wavelength light penetrates into tissue farther than other wavelengths due to tissue's low absorption in the NIR. To further increase the penetration of detected light, polarization £lters are used to selectively £lter light that has only scattered a few times. Thus light scattered from shallow tissue and generally corresponding to very short photon path lengths in the tissue are blocked whereas the more scattered light depolarizes and is detected.

The data from our imager are used to reconstruct local variations in the concentrations of analytes such as oxy- and deoxy-hemoglobin in the skin. This imager has been

used on patients with Kaposi's Sarcoma (KS) who are starting anti-angiogenesis therapy and then again at treatment week 42. In addition to the six NIR wavelengths, a three color visible photo is taken of the lesion site. The visible wavelength photos are used to correlate features such as tumor size as seen by the physician with our other data. Two infrared (IR) images are taken (3-5 micron and 8-12 micron) of the patient, as well laser Doppler images (LDI) at two wavelengths (670 nm and 780 nm). The IR images are designed to capture the thermal signature of the high blood ¤ow associated with angiogenesis. LDI measures the net blood velocity of the small blood vessels in tissue and generally increases as blood supply demands increase such as during angiogenesis.

We are interested in reconstructing tissue parameters that are correlated with cancer. Since the patients in this study are being treated with anti-angiogenesis drugs, parameters directly related to angiogenesis are desired. Blood volume is generally believed to increase during angiogenesis and is therefore of direct interest. Further, changes in blood oxygenation can be correlated to tumor metabolic activity. Thus, the two parameters of greatest interest to us are tissue blood volume and blood oxygen saturation. This paper describes preliminary results reconstructing relative spatial tissue blood volume and blood oxygen saturation values as indicators of tumor angiogenesis and tumor metabolism. These results are compared to our IR and LDI data.

2 Theory

We may assume that the absorption of blood is a function of the volume fraction of oxy- and deoxy-hemoglobin, V_{oxy} and $1 - V_{oxy}$ respectively. The relative absorption spectra for each type of hemoglobin $\mu_{a(oxy)}(\lambda)$ and $\mu_{a(deoxy)}(\lambda)$ are shown in Figure 1 [4]. The total blood absorption $\mu_{a(blood)}(\lambda)$ may be expressed as a combination of the two:

$$\mu_{a(blood)}(\lambda) = V_{oxy}\mu_{a(oxy)}(\lambda) + (1 - V_{oxy})\mu_{a(deoxy)}(\lambda) \quad (1)$$

Each of the band-pass £lters on the imager has a full width at half max (fwhm) of 50 nm. Before using the absorption data for reconstruction, the data must be convolved with the response function of the band-pass £lters. This smooths the data and removes much of the detail, particularly the deoxy response near 760 nm shown in Figure 1.

For light to reach the tumor it must pass through the epidermis. This transmission can be shown to be a function of the melanin in the epidermis and the epidermal thickness. The absorption spectrum for melanin $\mu_{a(mel)}(\lambda)$ is shown in Figure 2 [2].

We combine all other skin analytes into a single absorption variable $\mu_{a(skin)}(\lambda)$ which is a function of wavelength as shown in Figure 3 [3]. The dominant chromophores in that spectrum are lipids and water.

Now that the absorption spectra of the various analytes have been de£ned, the total absorption in the epidermis may be expressed as:

$$\mu_{a(epi)}(\lambda) = V_{mel}\mu_{a(mel)}(\lambda) + (1 - V_{mel})\mu_{a(skin)}(\lambda) \quad (2)$$

where V_{mel} is the volume fraction of melanin.

The epidermis is typically 0.1 mm thick which is approximately the mean scattering distance of photons in tissue. Scattering in tissue is typically very anisotropic with $g \approx 0.9$. This means that the few epidermal scatterings will typically be shallow angle and the transmission through the layer may be considered to be independent of scattering. The intensity after passage through the epidermis is:

$$I_{epi}(\lambda) = I_s(\lambda)e^{-\mu_{a(epi)}(\lambda)t} \quad (3)$$

where I_s is the intensity of our collimated light source and t is the epithelial thickness. In practice, the air-tissue interface will have a specular re¤ection. To address this, the source and detector have cross polarized £lters to block specularly re¤ected photons. We also assume that this £lter will block back-re¤ected photons that are scattered in the epidermis. In practice, these two components are accounted for by a scalar intensity scaling factor in the model.

The underlying dermis is where the tumor and blood vessels are located. This layer may be assumed to be in£nitely thick and the light passing from the epidermis is no longer collimated due to epidermal scattering. The re¤ected intensity from the dermis is [1]:

$$I_{ref}(\lambda) = I_{epi}\frac{1 - e^{\sqrt{24\mu_{a(derm)}(\lambda)/\mu_s{}'(\lambda)}}}{\sqrt{24\mu_{a(derm)}(\lambda)/\mu_s{}'(\lambda)}} \quad (4)$$

where

$$\mu_{a(derm)}(\lambda) = V_{blood}\mu_{a(blood)}(\lambda) + (1 - V_{blood})\mu_{a(skin)}(\lambda) \quad (5)$$

and $\mu_s{}'(\lambda)$ is the transport-corrected scattering coef£cient which is shown in Figure 4. Equation 5 is the integrated intensity over the entire plane for point illumination. In practice, we are looking at intensities at single pixels given illuminance over the entire plane.

We may then express the intensity detected by a camera as follows:

$$I_{detected}(\lambda) = cI_s(\lambda)d(\lambda)2I_{epi}(\lambda)I_{ref}(\lambda) \quad (6)$$

where $d(\lambda)$ is the spectral response of the camera. The product of $d(\lambda)$ and $I_x(\lambda)$ is generally combined into a single calibration function for the imaging device. This leaves an intensity scaling variable c which we reconstruct.

Equation 6 contains £ve variables, V_{oxy}, V_{blood}, V_{mel}, c, and t, that we wish to reconstruct. The six spectral bands

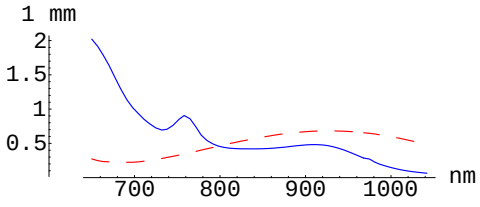

Figure 1. Absorption coef£cient for oxy-hemoglobin, $\mu_{a(oxy)}$, (dashed red) and deoxy-hemoglobin, $\mu_{a(deoxy)}$, (solid blue) shown as a function of wavelength

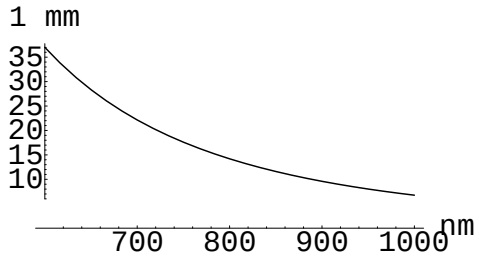

Figure 2. Melanin absorption coef£cient, $\mu_{a(mel)}$, as a function of wavelength

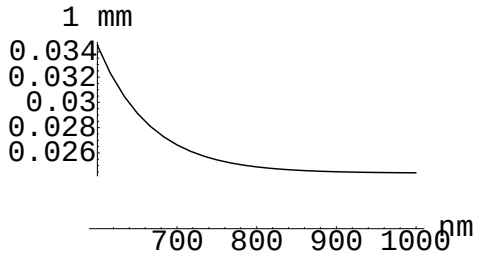

Figure 3. Skin absorption coef£cient, $\mu_{a(skin)}$, as a function of wavelength

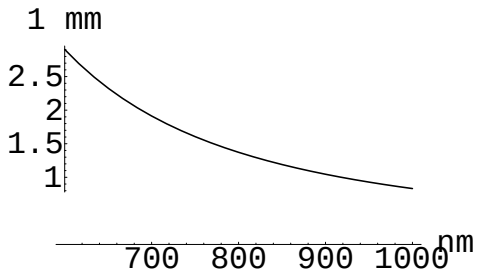

Figure 4. Transport-corrected scattering coef£cient coef£cient, μ_s', as a function of wavelength

of our imaging system allow for the reconstruction of up to six unknowns. The biggest source of error in Equation 6 is related to the change in μ_s' as function of wavelength. The change in pathlength is accounted for in Equation 4, but as μ_s' decreases, the volume sampled by the photons increases. Since the tissue has both physical and biophysical structures, changing the sampling volume with wavelength changes the actual concentrations of sampled analytes as a function of wavelength. As a result, it is impossible to quantitatively reconstruct analyte concentrations in heterogeneous tissues. We will instead look at relative differences in reconstructed analyte concentration as a potential indicator of disease status.

3 Results

To test the analysis, data were taken from a normal volunteer before and at the end of a £ve minute occlusion. The occlusion was created by application of a blood-pressure cuff that cut off all blood circulation to the arm. The data was analyzed for relative melanin content, epithelial thickness, blood volume and blood saturation as described previously. A location in the image sequence was picked that contains a blood vessel. The vein has low oxygen content and high blood volume as seen in Figure 5. Multiple-parameter plots containing combinations of high blood volume and low and high saturation are shown in Figure 6 where the vessel shows as high volume and low saturation and the surrounding tissue has high volume and saturation.

At the end of the occlusion, tissue blood volume had decreased by over a factor of 100 (0.058 to 0.00026) as shown in Figure 7. No evidence of the vessel is observable in the multiple parameter plots in Figure 8. It is not clear why the occlusion causes such a dramatic reduction in reconstructed blood volume when an increase in volume might be expected. Further, the change in oxy-hemoglobin was less than two percent (0.928 to 0.914). This experiment shows the trend that might be expected for a metabolically active tumor that was depleting its blood oxygen (even though the response indicates a reduction in blood volume which wouldn't be expected for angiogenesis) and this pattern re-emerges in the patient cases.

Patient 1 was imaged before the start of treatment and, as expected for a metabolically active tumor, has generally low reconstructed blood saturation in the tumor region as shown in Figure 9. The blood volume reconstructs low and the multiple parameter plots show the tumor with a similar combined response (Figure 10) as when the blood circulation is occluded in the normal patient (Figure 8). The normal tissue surrounding the patient's tumor reconstructs as high blood volume and saturation as seen in Figure 10.

Similar to patient 1, patient 2, also before the start of treatment, shows generally low reconstructed blood saturation in the tumor region and low blood volume in Figure 11.

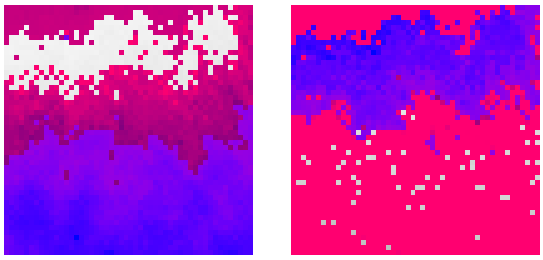

Figure 5. Normal patient reconstructed blood volume (left plot) and blood oxygen saturation (right plot) showing vein crossing top of image (blue is low, purple indicates mean values and red indicates high values)

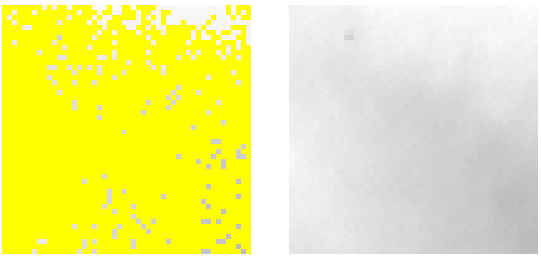

Figure 8. Normal patient at end of 5 min occlusion shows low blood volume and high saturation (yellow in left plot) and no high blood volume and oxygen saturation areas (red in right plot)

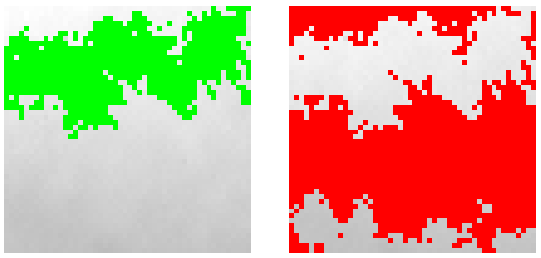

Figure 6. Normal patient showing regions of high blood volume and low saturation (green in left plot) and high volume, high saturation (red on right plot)

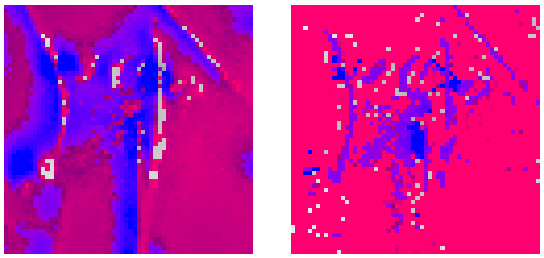

Figure 9. Patient 1 (pre-treatment) showing low blood volume (left plot) and generally lower saturation in the tumor region (right plot)

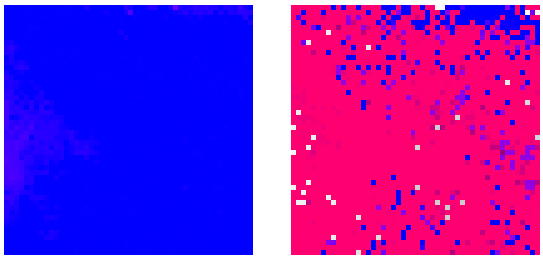

Figure 7. Normal patient at end of 5 min occlusion shows low blood volume (left plot) and no contrast in either plot (blood oxygen level on right) at the location of vessel as was seen in Figure 5

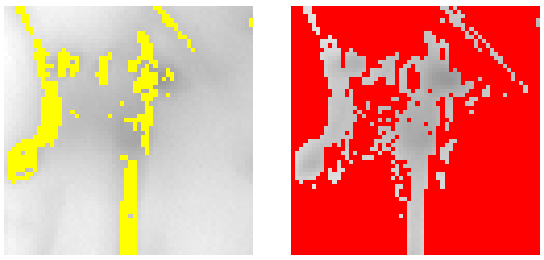

Figure 10. Patient 1 (pre-treatment) showing relatively combined low blood volume and saturation in tumor region (left plot) and high blood volume and saturation in the surrounding normal tissue (right plot)

The multiple parameter plots show the tumor with a similar combined response of low blood volume and saturation and the normal tissue surrounding the tumor reconstructs as high blood volume and saturation (Figure 12).

Patients 1 and 2 also show a similar band of low reconstructed melanin content around the edge of the tumor which is shown in Figure 13. This is believed to be an artifact caused by the non-uniform sampling volume of the photons at the different wavelengths. Since the tissue is particularly inhomogeneous at the tumor edge, this is where such artifacts are most likely.

Patient 1 has both a thermal and LDI signature at the tumor site as seen in Figures 14 and 15. In contrast, patient 2 has a relatively cool thermal signature at the tumor site (Figure 16) and no sign of the tumor in the LDI data.

Patients 3 and 4 are imaged with this device for the £rst time at week 42 of their treatment. The contrast for the blood saturation is similar to patients 1 and 2 as seen in Figures 17 and 18. What is signi£cant is that the mean reconstructed blood oxygen saturation of patients 3 and 4 (0.902 and 0.878 respectively) is much lower than for the normal volunteer and patients 1 and 2 (0.928, 0.959 and 0.954 respectively). As stated previously, the reconstructed values are not necessarily quantitatively correct, but the difference of 0.02 to 0.07 between the normal, and pre-drug patients and the patients at week 42 of anti-angiogenesis drug treatment appears signi£cant and may be an indication of the effect of the drug treatment.

Patient 3 has a particularly interesting pattern in the reconstructed blood volume values (Figure 17). Clearly the tumor has a bilateral asymmetry that may be indicative of some underlying process. The asymmetry also shows in the low volume, low saturation multiple parameter plot in Figure 19. The normal tissue, however, is still shown by the high volume, high saturation plot.

Patient 4 shows a more typical response in the multiple parameter plots with a good outline of the tumor region in the low volume high saturation plot and the normal tissue in the high volume high saturation plot as shown in Figure 20.

The outline of the tumor may also be clearly seen in the melanin reconstruction plots for both patients 3 and 4 in Figures 21 and 22.

Patients 3 and 4 have no LDI signature at the tumor site. There is a thermal signature at the site of patient 4's tumor.

4 Conclusion and Future Directions

Quanti£cation of analyte concentrations is very dif£cult, if not impossible, in heterogeneous tissue due to volume sampling changes at different wavelengths. The relative reconstructed values, however, have some utility in showing spatial patterns of analyte concentration that correlate with the tumor region.

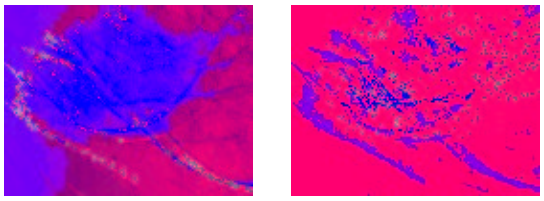

Figure 11. Patient 2 (pre-treatment) showing low blood volume (left plot) and generally lower saturation in the tumor region (right plot)

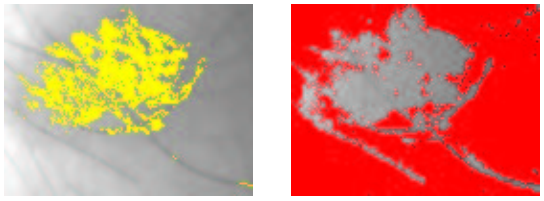

Figure 12. Patient 2 (pre-treatment) showing relatively combined low blood volume and saturation in tumor region (left plot) and high blood volume and saturation in the surrounding normal tissue (right plot)

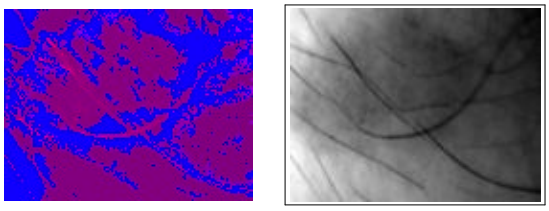

Figure 13. Patient 2 (pre-treatment) showing low reconstructed melanin band around edge of tumor (left plot) and 700 nm image (right plot) for comparison

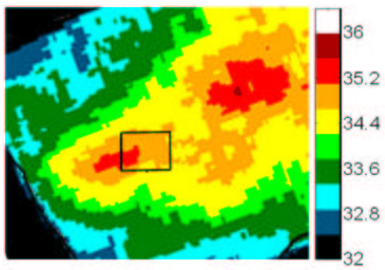

Figure 14. Patient 1 thermal image with black box showing tumor area

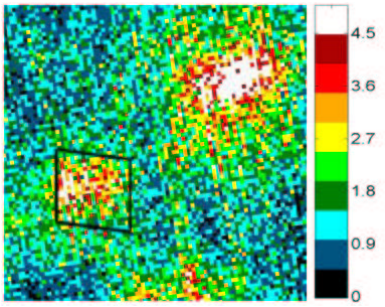

Figure 15. Patient 1 LDI image with black box showing tumor area

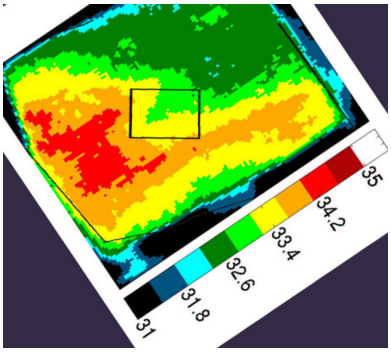

Figure 16. Patient 2 thermal image with black box showing tumor area

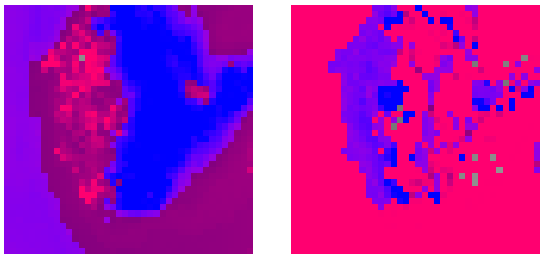

Figure 17. Patient 3 (week 42) showing generally lower saturation in the tumor region (right plot), but the left side of the tumor has higher blood volume (left plot)

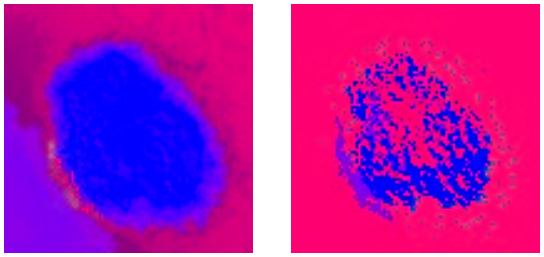

Figure 18. Patient 4 (week 42) showing low blood volume (left plot) and generally lower saturation in the tumor region (right plot)

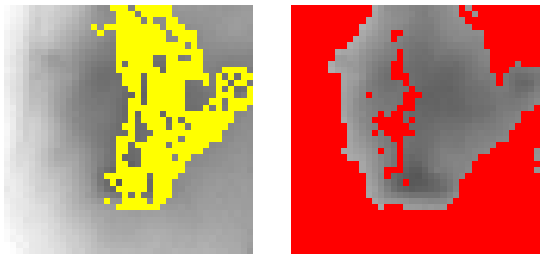

Figure 19. Patient 3 (week 42) showing relatively combined low blood volume and high saturation in tumor region (left plot) and high blood volume and saturation in the surrounding normal tissue (right plot)

The low reconstructed relative blood oxygen saturation values at the tumor site are expected for a metabolically active tumor that is placing demands on its blood supply. Angiogenesis processes in a tumor are expected to increase net blood volume in a tumor. The low relative reconstructed blood volume values may stem from a lack of penetration into the more blood perfused tumor tissue. Since blood is supplied from deep tissue, the surface tissue may have a relatively lower blood volume. This explanation, however, needs further investigation. The multiple parameter plot pixels with relatively high blood volume and saturation virtually always correspond to normal tissue and the low volume, high saturation pixels seem to correspond to tumor regions. The high saturation here is based on an average value within the imaged volume and does not contradict the fact that the tumor region is generally at a lower reconstructed saturation level than surrounding tissue.

This initial analysis of spectral information from patients suggests several areas for work to both improve the results and understand the observed patterns. The strength of the signal in the 750 to 800 nm range indicates that subdividing that interval is possible without loss of acquisi-

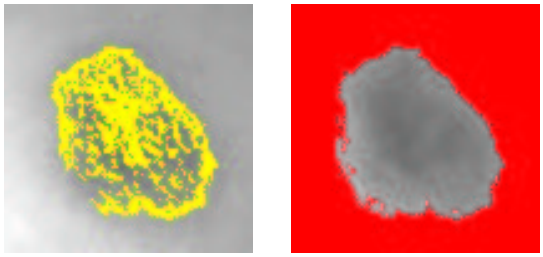

Figure 20. Patient 4 (week 42) showing relatively combined low blood volume and high saturation in tumor region (left plot) and high blood volume and saturation in the surrounding normal tissue (right plot)

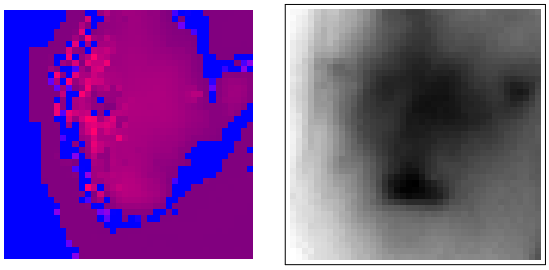

Figure 21. Patient 3 (week 42) showing low reconstructed melanin band around edge of tumor (left plot) and 700 nm image (right plot) for comparison

tion speed. This will provide a better discrimination of the blood saturation by amplifying the effect caused by the distinctive deoxy hemoglobin peak around 760nm. Removing the 1000 nm band where scattering is lowest will improve performance by reducing the differential in sampling volume over the acquired wavelengths.

The source of the band of low reconstructed melanin concentration around the edge of tumors is an area for additional research. First, a look at blemishes where differential melanin content is know to exist is warranted. Another possibility is that a similar, non-melanin chromophore associated with biochemistry at the tumor edge is responsible for the pattern. If turns out to be the case, a change to the model will be required for more realistic reconstructions. This edge contrast, however, may be useful in of itself as a marker of disease depending on the results of non-tumor blemish imaging.

It is believed that including lipids and water as separate analytes in the model will improve reconstruction accuracy since it is known that the concentration of these analytes in tumors is different than that in surrounding tissue. Despite

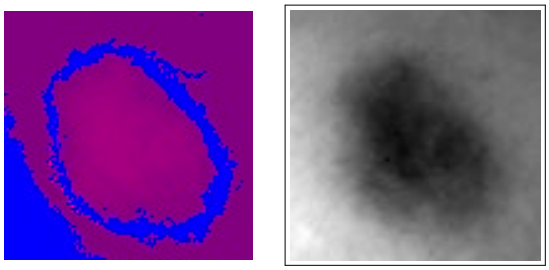

Figure 22. Patient 4 (week 42) showing low reconstructed melanin band around edge of tumor (left plot) and 700 nm image (right plot) for comparison

the fact that quantitative reconstruction of tumor properties may be impossible, clinically useful information appears to be contained in the relative spatial changes in reconstructed analyte concentrations.

References

[1] A. H. Gandjbakche and G. H. Weiss. Random walk and diffusion-like models of photon migration in turbid media. In E. Wolf, editor, *Progress in Optics*, volume 34, chapter 4, pages 333–402. Elsevier, Amsterdam, 1995.

[2] S. L. Jacques and D. J. McAuliffe. The melanosome: threshold temperature for explosive vaporization and internal absorption coef£cient during pulsed laser irradiation. *Photochemistry and Photobiology*, 53:769–775, 1991.

[3] I. S. Saidi, S. L. Jacques, and F. K. Tittle. Mie and Rayleigh Modeling of Visible-light Scattering in Neonatal Skin. *Applied Optics*, 34(31):7410–7418, 1995.

[4] S. Wray, M. Cope, D. T. Delpy, J. S. Wyatt, and E. O. R. Reynolds. Characterization of the near infrared absorption spectra of c ytochrome aa3 and haemoglobin for the noninvasive monitoring of cerebral oxygenation. *Biochimica et Biophsica Acta*, 933:184–192, 1988.